MET is required for the recruitment of anti-tumoural neutrophils

MET is required for the recruitment of anti-tumoural neutrophils

Veronica Finisguerra[1,2], Giusy Di Conza[1,2], Mario Di Matteo[1,2], Jens Serneels[1,2], Sandra Costa[1,2,3,4], A.A. Roger Thompson[5], Els Wauters[6,7,8], Sarah Walmsley[5], Hans Prenen[9], Zvi Granot[10], Andrea Casazza[1,2,§] & Massimiliano Mazzone[1,2,§]

[1]Laboratory of Molecular Oncology and Angiogenesis, Vesalius Research Center, VIB, Leuven, B3000, Belgium; [2]Laboratory of Molecular Oncology and Angiogenesis, Vesalius Research Center, Department of Oncology, KU Leuven, Leuven, B3000, Belgium; [3]Life and Health Sciences Research Institute (ICVS), School of Health Sciences, University of Minho, 4710-057 Braga, Portugal; [4]ICVS/3B's - PT Government Associate Laboratory, 4710-057 Braga/Guimarães, Portugal; [5]Department of Infection and Immunity, University of Sheffield, Sheffield S10 2RX, UK; [6]Respiratory Division, University Hospital Gasthuisberg, Leuven, B3000 Belgium; [7]Laboratory of Translational Genetics, Vesalius Research Center, VIB, Leuven, B3000, Belgium; [8]Laboratory of Translational Genetics, Vesalius Research Center, Department of Oncology, KU Leuven, Leuven, B3000, Belgium; [9]Digestive Oncology Unit, University Hospital Gasthuisberg, Department of Oncology, KU Leuven, Leuven, B3000 Belgium; [10]Department of Developmental Biology and Cancer Research, The Institute for Medical Research Israel-Canada, Jerusalem, 91120 Israel; § Editorial correspondence to massimiliano.mazzone@vib-kuleuven.be and andrea.casazza@vib-kuleuven.be

Running title: MET in neutrophils

Mutations or amplification of the *MET* proto-oncogene are involved in the pathogenesis of several tumours[1-4], which rely on the constitutive engagement of this pathway for their growth and survival[1,5]. For this reason, many preclinical and clinical studies have tested the efficacy of MET inhibition in cancer[1,6]. However, *MET* is expressed not only by cancer cells but also by tumour-associated stromal cells although its precise role in this compartment is not well characterized[7-12]. Here, we show that MET is required for neutrophil chemoattraction and cytotoxicity in response to its ligand HGF. Genetic deletion of *Met* in neutrophils enhances tumour growth and metastasis. This phenotype correlates with reduced neutrophil infiltration to both primary tumour and metastatic site. Similarly, *Met* is necessary for neutrophil transudation during colitis, skin rash or peritonitis. Mechanistically, *Met* is induced by tumour-derived TNF-α or other inflammatory stimuli in both mouse and human neutrophils. This induction is instrumental for neutrophil transmigration across an activated endothelium and iNOS production upon HGF stimulation. Consequently, HGF/MET-dependent nitric oxide release by neutrophils promotes cancer cell killing, which abate tumour growth and metastasis. Following systemic administration of a MET kinase inhibitor, we prove that the therapeutic benefit of MET targeting in cancer cells is partly countered by the pro-tumoural effect rising from MET blockade in neutrophils. Our work identifies an unprecedented role of MET in neutrophils, suggests a potential "Achilles' heel" of MET-targeted therapies in cancer, and supports the rationale for evaluating anti-MET drugs in certain inflammatory diseases.

To ensure specific deletion of *Met* in the immune system only, we took advantage of the Tie2:Cre deleter that excises floxed genes in both bone-marrow (BM) and endothelial cells (EC)[13] and we reconstituted lethally irradiated C57BL/6 wild-type (WT) mice with BM cells from Tie2;$Met^{wt/wt}$ (WT) or Tie2;$Met^{lox/lox}$ (KO) mice (Extended Data Fig. 2a), producing WT→WT or

KO→WT mice, respectively. When LLC lung carcinoma cells were injected subcutaneously, tumour volume, tumour weight, lung metastasis, total metastatic area and metastatic index were all higher in KO→WT than in WT→WT mice (Fig. 1a-g). KO→WT mice displayed reduced tumour apoptosis and necrosis, but increased proliferation (Extended Data Fig. 2b-n). Tumour vessel area, density, perfusion and oxygenation were instead similar in both chimeric mice (Extended Data Fig. 2o-r). A similar induction in tumour growth and metastasis was observed in non-irradiated KO versus WT mice (Extended Data Fig. 2s-u), but WT→KO chimeras displaying deletion of *Met* in EC only showed comparable tumour growth (and vascular features) to those observed in WT→WT controls (Extended Data Fig. 2o-r,v). Thus, gene inactivation of *Met* in immune cells favours cancer growth and metastasis.

Blood counts and percentage of circulating blood cell subsets did not change in WT→WT and KO→WT mice, either at baseline or upon LLC tumour engraftment (Extended Data Fig. 3a-e; Extended Data Table 1,2). Notably, KO→WT mice displayed reduced numbers of tumour-infiltrating $CD45^+$ leukocytes (Extended Data Fig. 3f,g) and, among all the different $CD45^+$ subpopulations, only $Ly6G^+$ tumour-associated neutrophil (TAN) accumulation was strongly reduced in KO→WT versus WT→WT mice at different time points (Fig. 1h-j; Extended Data Fig. 3f-k). Similarly, lungs from KO→WT tumour-bearing mice contained fewer $CD45^+$ leukocytes with decreased $Ly6G^+$ neutrophil infiltration, while macrophages were comparable (Fig. 1k-m; Extended Data Fig. 3l,m). Furthermore, reconstitution of *Met* in neutrophils only[14] (Extended Data Fig. 4a,b; Supplementary Table 1), was *per se* sufficient to rescue their recruitment and to hinder tumour growth and metastasis in KO→WT mice (Fig. 1n-q). *Vice versa*, restricted deletion of *Met* in neutrophils (Mrp8;$Met^{lox/lox}$) by means of the neutrophil-specific Mrp8:Cre line[14] (Extended Data Fig. 4c,d) recapitulated the accelerated growth and increased lung dissemination of subcutaneous LLC tumours observed in KO→WT chimeras, with marked TAN reduction as well (Fig. 1r-u;

Extended Data Fig. 4e). These results prove that MET is required for the recruitment of anti-tumoural neutrophils.

To extend our findings to other tumour types, we proved that *Met* deletion in the hematopoietic system increased the growth of *i)* orthotopic T241 fibrosarcomas and B16F10 melanomas, *ii)* spontaneous mammary tumours in MMTV-PyMT^{+} transgenic mice, *iii)* H-Ras^{G12V} and c-Myc-driven hepatocellular carcinomas (HCC), and *iv)* chemically induced colorectal cancers (CRC) (Fig. 2a-j; Extended Data Fig. 5a,b). Furthermore, the seeding capacity of B16F10 melanoma cells to the lungs (from either the primary tumour or after cancer cell intravenous injection) and of MMTV-PyMT^{+} breast tumours was boosted in *Met* KO chimeras (Fig. 2k,l; Extended Data 5c). In all these tumour types, *Met* KO TANs were fewer than WT TANs (Fig. 2m; Extended Data 5d,e). Interestingly, during chronic bowel inflammation, that precedes CRC formation, neutrophil but not macrophage infiltration of the colon was also abated by hematopoietic *Met* deletion, but this reduction did not impinge on colitis severity (Extended Data 5f-i). B16F10 and HCC displayed enhanced tumour growth (and metastasization) as well as reduced TAN infiltration in Mrp8;*Met*$^{lox/lox}$ versus Mrp8;*Met*$^{wt/wt}$ mice (Fig. 2n-q). Conversely, orthotopic Panc02 carcinomas grew and metastasized similarly in both WT→WT and KO→WT mice, and TAN infiltration did not change (Extended Data Fig. 5j-l). However, these tumours produced very little HGF compared to LLC tumours (Extended Data Fig. 5m,n). In general, plasma and intratumour HGF did not differ between genotypes (Extended Data Fig. 5o,p). In sum, *Met* deficiency in neutrophils promotes the progression of different (HGF-secreting) tumours.

Systemic treatment of WT mice carrying B16F10 melanomas (which are highly dependent on MET[15,16]) with three different MET tyrosine-kinase inhibitors (INCB28060, PF-04217903 or JNJ-38877605), strongly reduced TAN recruitment (Extended Data Fig. 5q). We then compared MET silencing in cancer cells versus systemic MET inhibition (Fig. 2r-t; Extended Data Fig. 5r).

PF-04217903 decreased weight and volume of B16F10 melanomas by 36% and 54% respectively, whereas MET knockdown in cancer cells by 58% and 75% (Fig. 2r,s). However, the combination of these two strategies was not synergic, but, on the contrary, dampened tumour inhibition to the same level as observed with PF-04217903 alone (Fig. 2r,s). TAN inhibition by PF-04217903 was comparable in both *Met*-silenced and scramble B16F10 melanomas (Fig. 2t). These data unveil how the therapeutic benefit of systemic MET inhibition is partly blunted by the blockade of anti-tumoural neutrophils.

To date, MET expression in neutrophils has been poorly documented[12]. We thus measured MET mRNA and protein levels in circulating or tumour-infiltrating neutrophils. Circulating $Ly6G^+$ cells from healthy mice expressed low levels of MET, but these levels were increased in circulating neutrophils from LLC tumour-bearing mice and even further in TANs (Fig. 3a,b; Extended Data Fig. 6a). Similarly, TANs isolated from non-small cell lung cancer patients displayed much higher *MET* levels than neutrophils isolated from healthy pulmonary tissue (Fig. 3c).

Co-culture with an IL-1α pre-activated endothelium as well as stimulation with tumour- or cancer cell-conditioned medium (TCM or CCM, respectively), potently induced MET transcript and protein in both mouse and human neutrophils (Fig. 3d-g). Screening for factors known to induce MET in other cells[17-19], we found that both TNF-α and LPS (but not IL-1α, HGF, or hypoxia) promoted MET expression in mouse and human neutrophils (Fig. 3h-k; Extended Data Fig. 6b-e; not shown). Particularly, TNF-α-mediated MET induction required TNFR1 and subsequent NF-κB activation (Fig. 3i-k). TNF-α alone was not able to trigger either MET phosphorylation or HGF release in neutrophils (Extended Data Fig. 6f-h).

Silencing of EC-borne TNF-α (which is 250-fold increased upon stimulation with IL-1α; Extended Data Fig. 6i), genetic knockout of neutrophil-borne TNFR1 (but not of TNFR2), or pharmacological blockade of TNF-α with the TNF-α-trap Enbrel, prevented *MET* induction in

mouse or human neutrophils upon co-culture with activated ECs or exposure to TCM/CCM (Fig. 3l; Extended Data Fig. 6j-m). Finally, systemic administration of Enbrel in LLC tumour-bearing mice diminished MET expression in neutrophils as well, resulting in their reduced recruitment to the tumour (Fig. 3m,n). Altogether, these data indicate that MET is scarcely expressed in naive neutrophils, but strongly induced by inflammatory stimuli.

Mechanistically, impaired TAN accumulation after *Met* inactivation was not due to a difference in apoptosis as assessed in vivo and in vitro, both at baseline and under LPS stimulation, with or without HGF (Extended Data Fig. 7a-e), but rather to a defect in neutrophil recruitment from the blood. Indeed, in case of acute inflammation, *Met* KO neutrophils displayed reduced exudation from circulation into the skin or into the peritoneal cavity (Fig. 4a-d; Extended Data Fig. 8a,b). Macrophage or lymphocyte recruitment did not change (Fig. 4d; Extended Data Fig. 8c,d). *Vice versa*, recombinant HGF was able to recruit $Ly6G^+$ cells inside a subcutaneous air pouch induced in WT mice, with similar efficacy of the neutrophil chemoattractant CXCL1 (Fig. 4e; Extended Data Fig. 8e). Instead, *Met* KO neutrophils did not migrate towards HGF, whilst their response to CXCL1 was preserved (Fig. 4e; Extended Data Fig. 8e). Mirroring this approach, systemic injection of an anti-HGF blocking antibody[20] prevented neutrophil infiltration to the tumour and to the inflamed skin (Fig. 4f).

We then tested in vitro the relevance of MET for neutrophil migration. Stimulation of WT neutrophils with HGF promoted their adhesion and chemotaxis through an activated endothelium whereas *Met* KO neutrophils (displaying 85% reduction in MET protein levels compared to WT; Extended Data Fig. 2a) completely lost this response (Fig. 4g,h; Extended Data Fig. 8f). In line with this, TCM (containing 2.6 ± 0.3 ng/ml HGF) promoted transendothelial migration of WT neutrophils, but its effect was 43% lower on *Met* KO neutrophils (Fig. 4i). Upon HGF neutralization, WT neutrophils responded to the TCM as *Met* KO neutrophils (Fig. 4i). HGF or

TCM did not influence neutrophil behaviour on non-activated ECs or on bare membranes (Extended Data Fig. 8f-h). Hence, HGF-mediated MET activation is required for neutrophil transendothelial migration to the inflammatory site.

Once migrated inside the tumour, N1 or N2 neutrophils can respectively inhibit or favour tumour progression[21]. Amongst the N1 and N2 genes, only the expression of the N1-type marker inducible nitric oxide synthase (*Nos2*, otherwise *iNos*) was lower in *Met* KO versus WT TANs but similar in macrophages (Fig. 4j; Extended Data Fig. 8i). Compared to WT→WT mice, tumours harvested from KO→WT mice displayed reduced nitric oxide (NO) production and 3-nitrotyrosine (3NT) formation, a sign of NO-mediated cell damage (Fig. 4k-n). In vitro, *Met* KO TANs had reduced cancer-cell-killing capacity than WT TANs; iNOS inhibition by L-NMMA blunted this difference (Fig. 4o; Extended Data Fig. 8j). Consistently, HGF stimulation of WT neutrophils (but not of *Met* KO neutrophils) promoted NO release and cytotoxicity, which was abated by L-NMMA (Extended Data Fig. 8k,l).

We then hypothesized that HGF/MET pathway is key for anti-tumoural neutrophils only. Indeed, neutrophil depletion in WT→WT chimeras did not affect significantly the growth of subcutaneous LLC tumours, implying that in this tumour model anti-tumoural and pro-tumoural neutrophils are in balance (Fig. 4p-r). In contrast, the same treatment in KO→WT mice reduced tumour growth by 34% (Fig. 4p-r), indicating that *Met* deletion inhibits recruitment and activation of cytotoxic, but not of pro-tumoural neutrophils, which are instead blocked by the anti-Ly6G antibody (Fig. 4r; Extended Data Fig. 8m).

In sum, we demonstrate that MET is induced by inflammatory stimuli. This receptor is then required for neutrophil extravasation to inflamed tissues. Once in the tissue, neutrophils respond to HGF by producing cytotoxic nitric oxide (Extended Data Fig. 1). All these steps restrain non-specific immune reactions to the inflammatory site and thus prevent the damage of healthy organs.

These findings highlight a double-edged role of MET in cancer: on one side, in MET-addicted tumours, this pathway is vital for cell-cycle and survival[2]; on the other side, it promotes anti-tumourigenic activities in neutrophils. Thus, alternative approaches targeting MET on cancer cells only, and trials guided by new patient selection strategies will be important to maximize the efficacy of MET inhibition in oncological diseases[3,4,22].

Finally, given the fact that MET-inhibiting drugs are not associated to overt toxicity[1,6], MET-targeted therapies might be exploited to ameliorate the symptoms of inflammatory disorders in which neutrophils are important effectors in the pathogenesis of these diseases[23].

REFERENCES

1 Gherardi, E., Birchmeier, W., Birchmeier, C. & Vande Woude, G. Targeting MET in cancer: rationale and progress. *Nat Rev Cancer* **12**, 89-103 (2012).

2 Bertotti, A. *et al.* Only a subset of Met-activated pathways are required to sustain oncogene addiction. *Sci Signal* **2**, ra80 (2009).

3 Lennerz, J. K. *et al.* MET amplification identifies a small and aggressive subgroup of esophagogastric adenocarcinoma with evidence of responsiveness to crizotinib. *J Clin Oncol* **29**, 4803-4810 (2011).

4 Choueiri, T. K. *et al.* Phase II and biomarker study of the dual MET/VEGFR2 inhibitor foretinib in patients with papillary renal cell carcinoma. *J Clin Oncol* **31**, 181-186 (2013).

5 Comoglio, P. M., Giordano, S. & Trusolino, L. Drug development of MET inhibitors: targeting oncogene addiction and expedience. *Nat Rev Drug Discov* **7**, 504-516 (2008).

6 Michieli, P. *et al.* Targeting the tumor and its microenvironment by a dual-function decoy Met receptor. *Cancer Cell* **6**, 61-73 (2004).

7 Bussolino, F. *et al.* Hepatocyte growth factor is a potent angiogenic factor which stimulates endothelial cell motility and growth. *J Cell Biol* **119**, 629-641 (1992).

8 Liu, Y. *et al.* Hepatocyte growth factor and c-Met expression in pericytes: implications for atherosclerotic plaque development. *J Pathol* **212**, 12-19 (2007).

9 Chen, Q., DeFrances, M. C. & Zarnegar, R. Induction of met proto-oncogene (hepatocyte growth factor receptor) expression during human monocyte-macrophage differentiation. *Cell Growth Differ* **7**, 821-832 (1996).

10 Baek, J. H., Birchmeier, C., Zenke, M. & Hieronymus, T. The HGF receptor/Met tyrosine kinase is a key regulator of dendritic cell migration in skin immunity. *J Immunol* **189**, 1699-1707 (2012).

11 Adams, D. H. *et al.* Hepatocyte growth factor and macrophage inflammatory protein 1 beta: structurally distinct cytokines that induce rapid cytoskeletal changes and subset-preferential migration in T cells. *Proc Natl Acad Sci U S A* **91**, 7144-7148 (1994).

12 Tesio, M. *et al.* Enhanced c-Met activity promotes G-CSF-induced mobilization of hematopoietic progenitor cells via ROS signaling. *Blood* **117**, 419-428 (2011).

13 Takeda, Y. *et al.* Macrophage skewing by Phd2 haplodeficiency prevents ischaemia by inducing arteriogenesis. *Nature* **479**, 122-126 (2011).

14 Elliott, E. R. *et al.* Deletion of Syk in neutrophils prevents immune complex arthritis. *J Immunol* **187**, 4319-4330 (2011).

15 Qian, F. *et al.* Inhibition of tumor cell growth, invasion, and metastasis by EXEL-2880 (XL880, GSK1363089), a novel inhibitor of HGF and VEGF receptor tyrosine kinases. *Cancer Res* **69**, 8009-8016 (2009).

16 Kishi, Y. *et al.* Systemic NK4 gene therapy inhibits tumor growth and metastasis of melanoma and lung carcinoma in syngeneic mouse tumor models. *Cancer science* **100**, 1351-1358 (2009).

17 Pennacchietti, S. *et al.* Hypoxia promotes invasive growth by transcriptional activation of the met protooncogene. *Cancer Cell* **3**, 347-361 (2003).

18 Moghul, A. *et al.* Modulation of c-MET proto-oncogene (HGF receptor) mRNA abundance by cytokines and hormones: evidence for rapid decay of the 8 kb c-MET transcript. *Oncogene* **9**, 2045-2052 (1994).

19 Dai, J. Y., DeFrances, M. C., Zou, C., Johnson, C. J. & Zarnegar, R. The Met protooncogene is a transcriptional target of NF kappaB: implications for cell survival. *J Cell Biochem* **107**, 1222-1236 (2009).

20 Suga, H. *et al.* IFATS collection: Fibroblast growth factor-2-induced hepatocyte growth factor secretion by adipose-derived stromal cells inhibits postinjury fibrogenesis through a c-Jun N-terminal kinase-dependent mechanism. *Stem Cells* **27**, 238-249 (2009).

21 Fridlender, Z. G. & Albelda, S. M. Tumor-associated neutrophils: friend or foe? *Carcinogenesis* **33**, 949-955 (2012).

22 Garber, K. MET inhibitors start on road to recovery. *Nat Rev Drug Discov* **13**, 563-565 (2014).

23 Wright, H. L., Moots, R. J., Bucknall, R. C. & Edwards, S. W. Neutrophil function in inflammation and inflammatory diseases. *Rheumatology* **49**, 1618-1631 (2010).

AUTHOR INFORMATION

Affiliations

[1]Laboratory of Molecular Oncology and Angiogenesis, Vesalius Research Center, VIB, Leuven, Belgium: V. Finisguerra, G. Di Conza, M. Di Matteo, J. Serneels, S. Costa, A. Casazza & M. Mazzone.

[2]Laboratory of Molecular Oncology and Angiogenesis, Vesalius Research Center, Department of Oncology, KU Leuven, Leuven, Belgium: V. Finisguerra, G. Di Conza, M. Di Matteo, J. Serneels, S. Costa, A. Casazza & M. Mazzone.

[3]Life and Health Sciences Research Institute (ICVS), School of Health Sciences, University of Minho, Braga, Portugal: S. Costa.

[4]ICVS/3B's - PT Government Associate Laboratory, Braga/Guimarães, Portugal: S. Costa.

[5]Department of Infection and Immunity, University of Sheffield, Sheffield, UK: R. Thompson & S. Walmsley.

[6]Respiratory Division, University Hospital Gasthuisberg, Leuven, Belgium: E. Wauters.

[7]Digestive Oncology Unit, University Hospital Gasthuisberg, Leuven, Belgium: H. Prenen.

[8]Department of Oncology, KU Leuven, Leuven, Belgium: H. Prenen.

[9]Department of Developmental Biology and Cancer Research, The Institute for Medical Research Israel-Canada, Jerusalem, Israel: Z. Granot.

Contribution

V.F performed experimental design, all experiments, data acquisition and interpretation. G.D.C performed in vitro assays, and measured tumour experiments. M.D.M performed ELISA assays, designed and performed cloning strategies. J.S. performed all the BMT and in vivo tumour experiments. R.T and S.W performed neutrophil isolations and peritonitis assays. Z.G. provided the *Mrp8* promoter. H.P provided data interpretation on the CRC and HCC models. A.C. performed experimental design, mouse tumour experiments, analysis of histological stainings and FACS, data acquisition and interpretation. M.M performed experimental design, data analysis, conducted scientific direction, wrote the manuscript.

Competing Financial Interests

No competing financial interests to declare.

Corresponding Author

Correspondence to: M. Mazzone (massimiliano.mazzone@vib-kuleuven.be) and A. Casazza (andrea.casazza@vib-kuleuven.be).

FIGURE LEGENDS

Figure 1. *Met* deficiency inhibits neutrophil recruitment to tumour and metastatic site

a-g, LLC tumour growth (**a**), weight (**b**), lung macrometastases (**c**), metastatic area (**d**) with representative images of H&E-stained lung sections (**e**,**f**), metastatic index (**g**) in WT→WT and KO→WT chimeras. Data combine 3 independent experiments; total mice: WT→WT=23, KO→WT=26. **h-m,** Neutrophil quantification and representative images on Ly6G-stained LLC tumour sections (**h-j**) or on lung sections from tumour-free and tumour-bearing mice (**k**), the latter represented in (**l**,**m**). Data in (**h**) are representative of 4 independent experiments (6-9 mice/condition per experiment). Data in (**k**) combine 2-3 independent experiments; total mice: Tumour-free=10/condition, Tumour-bearing=15/condition. **n-q,** LLC tumour growth (**n**), tumour weight (**o**), lung macrometastases (**p**), TAN quantification (**q**) in WT→WT or KO→WT chimeras reconstituted with *Met* in neutrophils only (Mrp8:Met); Mrp8:Empty is used as control. Data combine 2 independent experiments; total mice=10/condition. **r-u,** LLC tumour growth (**r**), tumour weight (**s**), lung macrometastases (**t**), TAN quantification (**u)** upon neutrophil-specific *Met* deletion (Mrp8;$Met^{lox/lox}$) and controls (Mrp8;$Met^{wt/wt}$). Data combine 2 independent experiments; total mice: Mrp8;$Met^{wt/wt}$=13, Mrp8;$Met^{lox/lox}$=14. *, P<0.05 versus WT→WT (**a-d**,**g**,**h**,**k**), versus Mrp8:Empty WT→WT (**n-q)**, versus Mrp8;$Met^{wt/wt}$ (**r-u**); #, P <0.05 versus Tumour-free (**k**), versus Mrp8:Empty KO→WT (**o,q**). Scale bars: 100 μm (**e,f**), 50 μm (**i,j,l,m**). All graphs show mean ± s.e.m..

Figure 2. *Met* deficiency in hematopoietic cells fosters progression of several tumour types

a-c, Tumor growth of T241 fibrosarcomas (**a**), B16F10 melanomas (**b**), PyMT-driven spontaneous multiple breast cancers (**c**). Data in (**a,b**) combine 2 independent experiments; total mice=14/condition (**a**), 8/condition (**b**). Data in (**c**) combine 3 independent experiments; total mice:

WT→PyMT=13, KO→PyMT=16. **d-g,** Liver weight (**d**), nodules (**e**), and images (**f,g**) after H-Ras^{G12V}/c-Myc-driven HCC (*n*=4 mice/condition). **h-j,** Quantification (**h**) on H&E-stained bowel sections (**i**,**j**) of AOM/DSS-induced colon adenomas (yellow arrowheads) or carcinomas (red arrowheads). Data combine 2 independent experiments; total mice=10/condition. **k,** Spontaneous lung metastases from B16F10 tumours or lung colonisation after B16F10 intravenous injection. Data combine 2 independent experiments; total mice=8/condition. **l,** Lung macrometastases from PyMT tumours. Data combine 3 independent experiments; total mice: WT→PyMT=13, KO→PyMT=16. **m**, TAN quantification in T241, B16F10, PyMT tumours, HCC, and CRC. Data combine 1-3 independent experiments; total mice: T241, CRC=10/condition, B16F10=8/condition, PyMT=13-16/condition, HCC=4/condition. **n,o,** B16F10 tumour growth (**n**), spontaneous metastases and lung colonisation (**o**) in Mrp8;*Met*$^{wt/wt}$ and Mrp8;*Met*$^{lox/lox}$ mice. Data combine 2 independent experiments; total mice: Mrp8;*Met*$^{wt/wt}$=12, Mrp8;*Met*$^{lox/lox}$=8. **p**, Liver nodules in Mrp8;*Met*$^{wt/wt}$ and Mrp8;*Met*$^{lox/lox}$ mice after H-Ras^{G12V}/c-Myc-driven HCC. Total mice=7/condition. **q**, TAN quantification in B16F10 tumours (total *n*: Mrp8;*Met*$^{wt/wt}$=12, Mrp8;*Met*$^{lox/lox}$=8) or HCC (total mice=7/condition). **r-t,** Tumour growth (**r**), weight (**s**) and TANs in *Met*-silenced (sh*Met*) B16F10 tumours after PF-04217903. Data combine 2 independent experiments (total mice=11-14/condition). *, P<0.05 versus WT chimeras (**a-e,h,k-m**), versus Mrp8;*Met*$^{wt/wt}$ (**n-q**), versus Scramble + Vehicle (**r**), versus its own Vehicle (**s,t**); #, P <0.05 versus Vehicles (**r**), versus Scramble (**s**). Scale bars: 200 μm (**i,j**), 0.5 cm (**f,g**). All graphs show mean ± s.e.m..

Figure 3. *Met* expression in neutrophils is induced by tumour-derived soluble factors

a-b, qRT-PCR (**a**) and FACS (**b**) analysis for MET in blood neutrophils from tumour (TM)-free or LLC-tumour-bearing mice and in TANs. **c,** qRT-PCR for *MET* in human neutrophils sorted from

lung cancer versus healthy tissue. *n*=4 patients. **d,e,** MET expression by qRT-PCR (**d**) or Western blot (**e**) in circulating neutrophils from tumour-free mice after co-culture with unstimulated (HUVEC/NS), IL-1α-pre-stimulated HUVEC (HUVEC/IL) or after stimulation with TCM or CCM. **f,g,** qRT-PCR (**f**) or Western blot (**g**) for MET in circulating human neutrophils after stimulation with A549-CCM. **h**, Western blot for MET in mouse and human neutrophils after LPS or TNF-α stimulation. **i,** qRT-PCR for *Met* in WT, TNFR1 KO or TNFR2 KO neutrophils after TNF-α stimulation. **j,k,** qRT-PCR (**j**) and Western blot (**k**) for MET in mouse neutrophils after TNF-α stimulation with or without NF-κB inhibitor. **l,** qRT-PCR for *Met* in mouse neutrophils co-cultured with HUVEC/IL or stimulated with TCM in presence or absence of the TNF-α trap Enbrel. **m,n,** FACS analysis for MET in TANs (**m**) and $Ly6G^+$ area (**n**) in LLC tumours after Enbrel. Data combine 2 independent experiments; total mice=5/condition. All data in (**a,b,d,f,i,j,l**) are representative of 2-3 independent experiments using 4-5 biological replicates/condition per experiment. All Western blots were repeated 2-3 times on independent biological replicates. Western blot full scan images are shown in Supplementary Figure 1. Loading control in (**e**,**h**) displays tubulin or actin according to Supplementary Figure 1. *, P <0.05 versus TM-free (**a**,**b**), versus Healthy lung (**c**), versus Mock (**d,f**), versus WT (**i**)**,** versus TNF-α (**j**)**,** versus IgG (**l-n**)**;** #, P <0.05 versus TM-bearing **(a,b**), versus Mock (**i**,**l**)**,** versus untreated **(j**). All graphs show mean ± s.e.m..

Figure 4. MET is required for neutrophil transendothelial migration and cytotoxicity

a-c, Neutrophils quantification (**a**) on TPA-painted ear skin (**b**,**c**). Data combine 2 independent experiments; total mice=6-9/condition. **d,** FACS analysis for Ly6G (neutrophils) or F4/80 (macrophages) on peritoneal lavages after zymosan-induced peritonitis. Representative of 2 independent experiments using 4-7 mice/condition per experiment. **e,** FACS analysis for neutrophil

recruitment towards HGF or CXCL1 in air pouch assays. Data combine 3 independent experiments; total mice=10/condition. **f,** Ly6G infiltration in LLC tumours or in TPA-painted ear skin after anti-HGF. Data combine 2 independent experiments; total mice: IgG=11, anti-HGF=6. **g-i,** Neutrophil adhesion to HUVEC/IL (**g**) and transendothelial migration in response to HGF (**h**) or TCM with or without anti-HGF (**i**). Representative of 3 independent experiments using 3 biological replicates/condition per experiment. **j,k**, qRT-PCR for *Nos2* in LLC-tumour-associated neutrophils or macrophages (**j**) and tumour-derived NO production (**k**). **l-n,** Quantification (**l**) and representative images (**m,n**) of 3NT- (green) and Ly6G- (red) costained LLC tumour sections. Data in (**j-n**) combine 2 independent experiments; total mice=8/condition. **o,** TAN cytotoxicity against LLC cells with or without L-NMMA. Representative of 4 independent experiments using 3 biological replicates/condition per experiment. **p-r,** LLC tumour growth (**p**), weight (**r**), TANs (**r**) following neutrophil-depleting anti-Ly6G. Data combine 2 independent experiments; total mice=16/condition.*, $P<0.05$ versus WT→WT in the same condition (**a,d,e,g-l,o-r**), versus IgG (**f**); #, $P<0.05$ versus Vehicle (**a**); versus PBS (**e**), versus Mock (**g-i**), versus WT→WT untreated (**o**), versus KO→WT IgG (**p,q**), versus IgG **(r**); $, $P<0.05$ versus WT→WT TCM (**i**). Scale bars: 100 μm (**b,c**), 20 μm (**m,n**). All graphs show mean ± s.e.m..

METHODS

Animals: The *Met* floxed mice, a gift of Dr. Thorgeirsson (NCI, Bethesda, MD), were backcrossed in a C57BL/6 background. The Tie2:Cre and MMTV-PyMT transgenic lines were obtained from our mouse facility. The Mrp8:Cre mice were a gift of Dr. Lowell (UCSF, San Francisco, CA) and Dr. Bruhns (Pasteur Institute, Paris, FR)[14,24-28]. C57BL/6 mice were purchased from Harlan. TNFR1 KO mice and TNFR2 KO mice were a gift of Dr. Libert (VIB, Ghent, BE). The *Met* floxed mice were intercrossed for at least two generations with Tie2:Cre or Mrp8:Cre in order to obtain $Met^{lox/lox}$ Cre negative (WT) or $Met^{lox/lox}$ Cre positive (KO) littermates for the specific promoter. All the experimental procedures were approved by the Institutional Animal Care and Research Advisory Committee of the KU Leuven. In all the experiments, mice were gender and age matched (within an age range between 6 and 10 weeks).

Bone marrow transplantation and blood cell count: Recipient 6-week old female mice were lethally irradiated (9.5 Gy) and then intravenously injected with 10^7 bone marrow (BM) cells from WT or KO mice 16 hours later. Experiments were initiated 5 weeks after BM reconstitution. Blood cell count was determined using a hemocytometer on peripheral blood collected by retro-orbital bleeding.

Hematopoietic stem/progenitor cell (HSPCs) transduction: For MET overexpression or reconstitution in respectively WT or *Met* KO neutrophils, lineage negative HSPCs were enriched with the mouse hematopoietic progenitor enrichment kit (Stem cell technologies) and checked for purity by FACS according to the manufacturer's protocol. $1x10^6$ cells/ml were pre-stimulated for 5 hours with stem span serum-free medium (Stem Cell Technologies) supplemented with IL-3 (20 ng/ml), SCF (100 ng/ml) TPO (100 ng/ml) and FLT-3L (100 ng/ml) (Promega) and transduced with $1x10^8$ TU/ml of a lentiviral vector expressing mouse *Met* under the promoter of the human gene *S100A8* (Mrp8:Met), which has been engineered for neutrophil-specific transcriptional targeting, or

an empty vector (Mrp8:Empty) as control. Briefly, the promoter driving *Met* expression in neutrophils only, corresponds to a 3.6 Kb DNA fragment encompassing the natural 5' and 3' regulatory regions but deleted of its exon coding sequences. Hence, *Met* is under the control of the 5' and 3' untraslated regions of the human *S100A8* gene and other proximal *cis* regulatory sequences present in the surrogate DNA fragment[14,24-28] . Ten hours after the first viral transduction, cells received a second round of their respective lentiviral vector; 7 hours later $1x10^6$ cells were injected via tail vein in lethally irradiated C57BL/6 recipient mice. A fraction of transduced HSPCs were cultured and collected after 9 days to measure the number of integrated vector copies/cell genome (vector copy number, VCN) by qPCR using custom TaqMan assays specific for HIV-gag sequences (Applied Biosystems), as previously described[29]. Standard curves for HIV-gag (contained by both Mrp8:Empty and Mrp8:Met lentiviral vectors) were obtained from the corresponding plasmids. Fifty ng of genomic DNA from each sample was subjected to qPCR in quadruplicate using an ABI Prism 7500 Fast Real-Time PCR System (Applied Biosystems). VCN was determined comparing the amplification signal on the genomic DNA with the standard curve consisting of serial dilutions over a 6 log range (slope ≈ -3,3, intercept ≈ 35, efficiency % ≈ 100). Average copies per cell genome were calculated taking into account that one murine diploid genome = 5,92 pg. The results of this analysis are shown in Supplementary Table 1.

Tumour models: $2x10^6$ LLC or $1x10^6$ B16F10 were injected subcutaneously while $2x10^6$ T241 cells were injected intradermally in a volume of 200 µl PBS. Tumour volumes were measured 3 times a week with a calliper. At endstage, tumours were weighed and collected for histological examination or FACS analysis. MMTV-PyMT$^+$ spontaneous breast tumours were measured 10 weeks after birth (6 weeks after BM transplantation), three times a week, and sacrificed at week 16. Lung metastases were contrasted by intratracheal injection of a 15% India ink solution, by hematoxylin eosin (H&E) staining on lung paraffin sections, or detected by qRT-PCR for the

melanoma-specific gene *S100B* in the models involving B16F10 cells. For orthotopic pancreatic tumour growth, mice were anesthetized with isoflurane, the stomach exteriorized via abdominal midline incision, and $1x10^6$ Panc02 tumour cells in 30 μl PBS were injected into the head of the pancreas using a 29-gauge needle. A successful intrapancreatic injection of tumour cells was identified by the appearance of a fluid bleb without intraperitoneal leakage. Mice displaying peritoneal leakage were immediately sacrificed and excluded from the analysis. At day 12, primary tumours were removed and weighed. Enlarged lymph nodes were counted under a stereoscopic microscope. For the chemically-induced colorectal cancer model, body-weight-matched mice received one intraperitoneal injection of 10 mg/kg of azoxymethane (AOM) followed by 3 cycles of 7 days of 1.5% (cycle I) or 1.7% (cycle II-III) dextran sodium sulphate (DSS) in drinking water, starting from the day of AOM injection[30]. After 160 days, the colon was collected and prepared for histological evaluation with the "Swiss roll" technique[31]. For the oncogene-driven hepatocellular carcinoma model, mice received a 1:1 molar ratio (3 μg total DNA) of piggyBac transposons encoding for c-Myc and H-Ras^{G12V} oncogenes, driven by the PGK promoter, together with the hyperactive piggyBac transposase-encoding plasmid[32]. DNA solutions containing transposon/transposase plasmids were diluted in 2 ml of Ringer's solution and hydrodynamically delivered in 7 seconds through the tail vein.

Mice treatments: To induce chronic colitis, mice received 3 cycles of 7 days of 1.5% (cycle I) or 1.7% (cycle II-III) dextran sodium sulphate (DSS) in drinking water; 2 weeks after the last DSS cycle, the colon was collected and prepared for histological evaluation as described above[31]. For in vivo MET inhibition, B16F10 tumour-bearing mice received 40 mg/kg PF-04217903 (AbMole Bioscience) or the corresponding vehicle (0.5% methylcellulose in saline) via oral gavage every day once a day starting from day 2 after tumour injection and twice a day from day 11 until the end of the experiment; alternatively mice were treated with 50 mg/kg INC280 (AbMole Bioscience) or

50 mg/kg JNJ-38877605 (Selleckchem). For TNF-α inhibition in vivo, LLC tumour-bearing mice were randomized for comparable tumour volumes at the endstage and i.p. injected with 10 mg/kg of Enbrel or human IgG in PBS, three and one day before tumour collection. For HGF inhibition in vivo, LLC tumour-bearing mice were randomized when average tumour volume was 300 mm^3 and i.p. injected with 0.2 mg/mouse of anti-HGF blocking antibody (AF-2207, R&D[20,33]) or goat IgG in PBS. Tumours were collected 20 hours later for histological analysis; TPA ear painting was done 5 hours after antibodies administration and ears were collected 15 hours later. For neutrophil depletion, mice were treated with 50 μg/20 g body weight of rat anti-mouse Ly6G antibody (clone 1A8, BioXCell) or rat IgG every second day starting from day 4 after LLC tumour injection and every day from day 12 after tumour injection until the end of the experiment. Efficiency of neutrophil depletion was assessed by FACS in blood and tumours.

TPA model of acute skin inflammation: Phorbol ester TPA was used to induce acute skin inflammation as described before[34]. Briefly, TPA (2.5 μg in 20 μl acetone per mouse) was topically applied on the ear skin of anaesthetized mice. The contralateral ear was painted with acetone alone as vehicle control. Mice were sacrificed after 24 hours and ears collected in 2% PFA for histological analysis.

Zymosan-mediated acute peritonitis model: To induce acute peritonitis, zymosan A (Sigma) was prepared at 2 mg/ml in sterile PBS. Four hours after i.p. injection of 0.1 mg zymosan A per mouse, inflammatory exudates were harvested by peritoneal lavage with 2 ml PBS. Cells were counted with a Burker chamber and stained for Ly6G (1A8) and F4/80 (BM8) for FACS analysis.

Air pouch assay: To create subcutaneous air pouches, BM transplanted chimeric mice or Mrp8;*Met*$^{lox/lox}$ or Mrp8;*Met*$^{wt/wt}$ mice were injected with 3 ml of sterile air by dorsal subcutaneous injection with a butterfly 23G needle on day 0 and on day 3. On day 6, 200 ng/mouse of murine CXCL1 or HGF dissolved in 0.5 ml PBS-Heparin (15 U/ml) or PBS-Heparin (15 U/ml) as control,

were injected in the newly formed dorsal camera. After 4 hours, inflammatory cells were harvested by washing the pouch with 5 ml of PBS. Cells were stained for Ly6G (1A8), washed and resuspended in PBS 0.1% BSA with unlabelled counting beads and quantified by FACS.

Mouse blood neutrophil isolation: Blood was collected from the retro-orbital vein in 10% heparin and diluted in an equal volume of PBS 0.5% BSA. Up to 5 ml of diluted blood was layered on top of a discontinuous gradient of Histopaque 1119 (4 ml) and Histopaque 1077 (5 ml) from Sigma. The gradient was centrifuged for 30 minutes at 700g with brake off. The neutrophil layer between the Histopaque 1077 and 1119 was collected and washed in PBS 0.5% BSA. RBC lysis was performed as in Supplementary Methods. Neutrophils were washed in PBS 0.5% BSA, counted and resuspended according to the experimental condition. Alternatively, blood was sedimented in a saline solution containing 1.25% dextran and neutrophils were negatively selected with magnetic beads[35]. Neutrophil purity, as assessed by the hemocytometer, was always higher than 93%.

Bone marrow neutrophil and mononuclear cell isolation: In order to reach reasonable amounts of protein, all the Western Blot analyses in mice were performed on neutrophils isolated from bone marrows. Mice were sacrificed by cervical dislocation. Femurs and tibias were collected in cold sterile Hank Balanced Salt Solution (HBSS, Invitrogen) and flushed with HBSS 0.25% BSA. Cells were layered on top of a discontinuous gradient of Percoll 81%, 62%, 55%, freshly prepared and centrifuged for 30 minutes at 2000 g with break off. Monocytes were collected at the interface between the BM cells and the layer of Percoll 55%, whereas neutrophils were collected at the interface between Percoll 55% and 62%. Cells were washed in HBSS 0.25% BSA and RBC lysis was performed as described above. Neutrophils (or monocytes) were washed again, counted and resuspended according to the experimental setting. Neutrophil (or monocyte) purity assessed by hemocytometer was higher than 87%.

FACS analysis and flow sorting of blood or tumour-associated cells: Blood was collected in 10% heparin and stained for 20 minutes at room temperature. After RBC lysis, cells were washed and resuspended in FACS buffer (PBS containing 2% FBS and 2 mM EDTA). Tumours were minced in RPMI medium containing 0.1% collagenase type I and 0.2% dispase type I (Gibco) for 30 minutes at 37°C and passed through a 70 and 40 μm cell strainer. After RBC lysis, cells were resuspended in FACS buffer and stained for 20 minutes at 4°C. Lungs were collected after 7 minutes of transcardial perfusion with saline and processed as for the tumours. Briefly, blood or single cell suspensions were incubated for 15 minutes at 4°C with Mouse BD Fc Block (2.4G2, BD Pharmingen) 1:100 in FACS buffer. The antibodies were added directly in the blocking solution in the appropriate combinations (as indicated in the figure legends). CD45 (30F-11), CD11b (M1/70), Ly6G (1A8), CD45R (RA3-6B2), CD3 (17A2), CD4 (RM4-5), IgE (R35-72), CD49b (DX5), Ly6C (AL-21) (all from BD Pharmingen), F4/80 (BM8), CD115 (AF598), MHCII (M5/114.15-12) (all from eBioscience), were used 1:200 for $2x10^6$ in 100 μl; Siglec-F (E50-2440, BD Pharmingen) was diluted 1:750. In all the stainings 7AAD (BD Pharmingen) was used to gate out dead cells. For intra-tumour proliferation, 1 mg of BrdU was i.p. injected in each mouse 4 hours before tumour collection and cell proliferation was quantified on single cell suspensions with the FITC BrdU Flow Kit (BD Bioscience) according to manufacturer's protocol. Tumour apoptosis was assessed by staining single cell suspension for the apoptotic marker AnnexinV (1:40, BD Bioscience), excluding 7AAD positive cells. For TAN apoptosis, tumour single cell suspensions were gated for CD11b (M1/70) and Ly6G (1A8); AnnexinV and 7ADD were used to distinguish apoptotic or dead neutrophils. In vitro neutrophil apoptosis was performed by seeding neutrophils isolated from tumour-bearing mice at a concentration of $1x10^6$/ml and stimulating them with or without LPS (1μg/ml), alone or in combination with HGF (100 ng/ml) for 10 h at 37°C. Cells were collected, washed and stained for AnnexinV and 7AAD. The combination of CD11b (M1/70), Ly6G (1A8)

and MET (eBioclone 7, eBioscience) was used to identified triple-positive MET expressing neutrophils in blood or tumour cells 7AAD-negative. Freshly stained samples were analysed by FACS Canto II (BD Bioscience). For tumour-associated neutrophil sorting, myeloid population was enriched by coating with CD11b-conjugated magnetic beads (MACS, Miltenyi Biotec) and separation through magnetic columns (MACS, Miltenyi Biotec), staining with Ly6G and sorting with a FACS Aria I (BD Bioscience). Cells were collected in RLT buffer (Qiagen) for RNA extraction or resuspended according to the experimental conditions.

Western blot: To assess MET deletion, BM cells, neutrophils, peritoneal macrophages, monocytes (all cultured overnight in TCM) or endothelial cells were lysed in hot Laemmli buffer (2.5% SDS, 25% Tris-HCl pH 6.8) for 10 minutes at 96°C, sonicated, cleared and quantified. Alternatively, $2x10^6$ bone marrow derived neutrophils from WT mice were stimulated with TCM, CCM, 100 ng/ml of murine TNF-α (or mock medium 0% FBS or 10% FBS as control) for 20 hours at 37°C. For the co-culture with HUVEC, a monolayer of HUVEC was stimulated for 4 hours with 5 ng/ml IL-1α at 37°C, and washed before neutrophil seeding. After 20 hours of stimulation, neutrophils were collected using Cell Dissociation Buffer Enzyme Free PBS-Based (Gibco). Cells were washed in PBS, lysed in 15 µl of a protease inhibitor mixture and incubated for 15 minutes on ice. The protease inhibitor mixture was obtained by dissolving one tablet of Complete Mini protease inhibitor mixture (Roche) in 5 ml of PBS with 2 mM diisopropyl fluorophosphate (DFP; Acros Organics, Morris Plains, NJ). After addition of an equal amount of 2x SDS sample buffer supplemented with 4% 2-mercaptoethanol, the lysates were boiled for 15 minutes and kept at −80°C until use. NF-κB inhibition was achieved by pre-treating $7x10^6$ neutrophils with 10 µM 6-amino-4-(4-phenoxyphenylethylamino) quinazoline (Calbiochem) for 1 hour at 37°C; cells were then stimulated with murine TNF-α (100 ng/ml) for 5 hours before lysis. Human MET was assessed by stimulating $3x10^7$ blood neutrophils isolated from the blood of healthy volunteers with A549-

CCM, 100 ng/ml human TNF-α, 50 ng/ml LPS (or mock medium 10% FBS as control) for 20 hours. Cells were incubated with 2.7 mM DFP for 15 minutes at 4°C, collected and washed in PBS supplemented with 2.7 mM DFP and Complete Mini protease inhibitor 1X, and lysed in hot Laemmli buffer at 96°C for 10 minutes. Cell lysates were sonicated, cleared and quantified. 6x loading buffer was added before loading on the gel. The following primary antibodies were used: mouse anti-mouse Met (3D4, Invitrogen), mouse anti-mouse β-actin (I-19, Santa Cruz), mouse anti-vinculin (hVIN-1, Sigma), rabbit anti-human Met (D1C2, Cell Signaling), HRP-conjugated anti-beta-tubulin (Abcam). The following secondary antibodies were used: HRP-conjugated goat anti-mouse and HRP-conjugated goat anti-rabbit (Santa Cruz). Signal was visualized by Enhanced Chemiluminescent Reagents (ECL, Invitrogen) or West Femto by Thermo Scientific according to the manufacturer's instructions.

Adhesion assay: $4x10^4$ HUVEC were seeded in M199 20% FBS in a 96-multiwell plate, previously coated with 0.1% gelatin. After 12 hours, HUVEC were stimulated with 5 ng/ml IL-1α in DMEM 10% FBS at 37°C. After 4 hours the endothelial monolayer was thoroughly washed and $2.5x10^5$ WBC isolated indistinctly from Tie2;*Met*$^{wt/wt}$ and Tie2;*Met*$^{lox/lox}$ mice or from WT→WT and KO→WT transplanted mice, were seeded on top of it, with or without murine HGF (50 ng/ml). After 15 minutes non-adherent cells were washed out whereas adherent cells were detached by using a Cell Dissociation Buffer Enzyme Free PBS-Based (Gibco). Cells were stained for Ly6G (clone 1A8), washed and resuspended in PBS-BSA 0.1% with unlabelled counting beads (BD Bioscience) and quantified by FACS Canto II (BD Bioscience).

Transmigration and migration assay: For the transmigration assay, $2x10^5$ HUVEC were seeded on 3 μm polycarbonate membrane (Transwell; Costar) previously coated with 0.1% gelatin in M199 20% FBS. After 12 hours, HUVEC were stimulated for 4 hours at 37°C in DMEM 10% FBS with 5 ng/ml IL-1α and then washed. $5x10^5$ WBC isolated indistinctly from Tie2;*Met*$^{wt/wt}$ and

Tie2;*Met*$^{lox/lox}$ mice or from WT→WT and KO→WT transplanted mice were seeded on top of the endothelial monolayer, while mock medium, TCM (with or without 3 μg/ml anti-HGF antibody AF-2207, R&D[33]) or 50 ng/ml murine HGF was added in the bottom. After 2 hours at 37°C, transmigrated cells were collected from the bottom chambers and from the lower side of the filter with cold PBS 0.5% EDTA. Cells were stained and Ly6G$^+$ cells quantified as above. In the migration assays WBC were seeded directly on top of 3 μm polycarbonate porous membranes.

Cytotoxicity assay: LLC sh*Met* or T241 sh*Met* were transduced with a luciferase-expressing lentiviral vector (EX-hLUC-Lv114 from GeneCopoeia); 10^4 cells were then seeded in DMEM 10% FBS in a 96-multiwell plate. After 4 hours, $0.2x10^6$ neutrophils purified from the blood of tumour bearing mice or directly from the tumours themselves, were co-cultured with the cancer cells in DMEM 2% FBS for 4 hours at 37°C, with or without 100 ng/ml mouse HGF or 1 mM L-NMMA (Sigma). After washing, adherent cells were lysate in 0.2% Triton, 1 mM DTT. Luciferase signal was revealed with a microplate luminometer. The use of sh*Met* was thought to prevent any possible confounding activity of MET on cancer cell survival and thus to restrict the effect of HGF to neutrophils only.

Statistics: Data entry and all analyses were performed in a blinded fashion. All statistical analyses were performed using GraphPad Prism software. Statistical significance was calculated by two-tailed unpaired t-test on two experimental conditions or two-way ANOVA when repeated measures were compared, with $P<0.05$ considered statistically significant. Data were tested for normality using the D'Agostino-Pearson omnibus test (for $n>8$) or the Kolmogorov-Smirnov test (for $n\leq 8$) and variation within each experimental group was assessed. Detection of mathematical outliers was performed using the Grubbs' test in GraphPad. Sample sizes for all experiments were chosen based on previous experiences. Independent experiments were pooled and analysed together whenever possible as detailed in figure legends. All graphs show mean values ± s.e.m.

24 Passegue, E., Wagner, E. F. & Weissman, I. L. JunB deficiency leads to a myeloproliferative disorder arising from hematopoietic stem cells. *Cell* **119**, 431-443 (2004).

25 Van Ziffle, J. A. & Lowell, C. A. Neutrophil-specific deletion of Syk kinase results in reduced host defense to bacterial infection. *Blood* **114**, 4871-4882 (2009).

26 Abram, C. L., Roberge, G. L., Pao, L. I., Neel, B. G. & Lowell, C. A. Distinct roles for neutrophils and dendritic cells in inflammation and autoimmunity in motheaten mice. *Immunity* **38**, 489-501 (2013).

27 Albanesi, M. *et al.* Neutrophils mediate antibody-induced antitumor effects in mice. *Blood* **122**, 3160-3164 (2013).

28 Lagasse, E. & Clerc, R. G. Cloning and expression of two human genes encoding calcium-binding proteins that are regulated during myeloid differentiation. *Mol Cell Biol* **8**, 2402-2410 (1988).

29 Hamm, A. *et al.* PHD2 regulates arteriogenic macrophages through TIE2 signalling. *EMBO Mol Med* **5**, 843-857, (2013).

30 Neufert, C., Becker, C. & Neurath, M. F. An inducible mouse model of colon carcinogenesis for the analysis of sporadic and inflammation-driven tumor progression. *Nat Protoc* **2**, 1998-2004 (2007).

31 Moolenbeek, C. & Ruitenberg, E. J. The "Swiss roll": a simple technique for histological studies of the rodent intestine. *Lab Anim* **15**, 57-59 (1981).

32 Chen, X. & Calvisi, D. F. Hydrodynamic transfection for generation of novel mouse models for liver cancer research. *Am J Pathol* **184**, 912-923 (2014).

33 Schira, J. *et al.* Significant clinical, neuropathological and behavioural recovery from acute spinal cord trauma by transplantation of a well-defined somatic stem cell from human umbilical cord blood. *Brain* **135**, 431-446, (2012).

34 Cramer, T. *et al.* HIF-1alpha is essential for myeloid cell-mediated inflammation. *Cell* **112**, 645-657 (2003).

35 Cotter, M. J., Norman, K. E., Hellewell, P. G. & Ridger, V. C. A novel method for isolation of neutrophils from murine blood using negative immunomagnetic separation. *Am J Pathol* **159**, 473-481 (2001).

Extended Data Figure 1. Scheme illustrating the role of MET in neutrophils.

During cancer or infections, the release of cytokines such as IL-1 at the inflammatory site will promote the expression of TNF-a on the endothelium and the surrounding tissue. When circulating neutrophils will encounter the activated endothelium, TNF-a will unleash NF-kB through the binding to TNFR1, which in turn will induce MET expression on neutrophil surface. HGF, also released and proteolytically activated at the site of inflammation, will bind to MET and stimulate the firm adhesion of neutrophils to the endothelium, likely via integrin engagement, and thus neutrophil diapedesis. Once extravasated, HGF/MET pathway will still function on neutrophils by reinforcing their cytotoxic response through the induction of iNOS and NO production, ultimately favouring a bactericidal and tumouricidal neutrophil phenotype.

Extended Data Figure 2. *Met* deletion in immune cells, but not in ECs, fosters tumour growth.

a, MET expression in total bone marrow (BM) cells, endothelial cells (ECs) and neutrophils harvested from *Met* floxed mice intercrossed with the Tie2:Cre deleter thus generating Tie2;$Met^{lox/lox}$ (KO) or Tie2;$Met^{wt/wt}$ (WT) mice. Western blots are representative of 3 repetitions on independent biological replicates. Western blot images have been cropped for presentation. Full scan images are shown in Supplementary Figure 1. **b-d,** Quantification (**b**) and representative images of tumour sections' TUNEL stainings (**c,d**) from subcutaneous endstage LLC tumours in WT→WT and KO→WT mice. Data combine 2 independent experiments; total *n*=10 mice/condition. **e**, FACS quantification of $AnnexinV^{+}$ $7AAD^{-}$ early apoptotic tumour cells in WT→WT and KO→WT mice. Data combine 2 independent experiments; total *n*=8 mice/condition. **f-j**, Tumour necrosis quantification in WT→WT and KO→WT mice (**f**), assessed by histologic evaluation of H&E stained tumour sections (**g**,**h**) and by measurement of autofluorescent tumour areas (**i,j**); yellow dotted lines demarcate necrosis. Data combine 2 independent experiments; total

n=10 mice/condition. **k-m**, Quantification (**k**) and representative images of tumour sections stained for the proliferation marker pHH3 (**l,m**) from subcutaneous endstage LLC tumours in WT→WT and KO→WT mice. Data combine 2 independent experiments; total *n*=10 mice/condition. **n**, FACS quantification of $BrdU^+$ proliferating tumour cells in WT→WT and KO→WT mice. Data combine 2 independent experiments; total *n*=10 mice/condition. **o-r**, $CD31^+$ vessel area (**o**), vessel density (**p**), lectin perfusion (**q**), and hypoxic ($Pimo^+$) area (**r**) in LLC subcutaneous tumours from KO→WT mice (where the hematopoietic/immune system is knocked out for *Met*) or WT→KO mice (where ECs only are knocked out for *Met*) compared to control WT→WT mice. Data in **o-r** combine 2 independent experiments; total *n*: WT→WT=12, KO→WT=8, WT→KO=8. **s-u**, Subcutaneous LLC tumour growth (**s**), weight (**t**) and lung metastases (**u**) in Tie2;$Met^{lox/lox}$ compared to Tie2;$Met^{wt/wt}$ mice. Data combine 2 independent experiments; total *n*: Tie2;$Met^{wt/wt}$=12, Tie2;$Met^{lox/lox}$=10. **v**, Tumour growth in endothelial cell specific *Met* KO (WT→KO) and control (WT→WT) mice. Data combine 2 independent experiments; total *n*=8/condition. *, $P<0.05$ versus WT→WT (**b,e,f,k,n)**, versus Tie2;$Met^{wt/wt}$ (**s-u)**. Scale bars: 50 μm (**c,d,l,m),** 100 μm (**g-j)**. All graphs show mean ± s.e.m.

Extended Data Figure 3. Circulating and tumour-infiltrating immune cells upon *Met* deletion.

a-e, FACS analysis showing percentages of circulating monocytes (**a**), lymphocytes (**b**), neutrophils (**c**), eosinophils (**d**), and basophils (**e**) in tumour free or in LLC-tumour bearing WT→WT and KO→WT mice. Data combine 2 independent experiments; total *n*=8 mice/condition. **f**, Quantification of LLC-tumour sections stained for the pan-leukocyte marker CD45, the macrophage marker F4/80, the NK marker NK1.1, the B lymphocyte marker CD45R, the T helper cell marker CD4, the cytotoxic T cell marker CD8 and the dendritic cell marker CD11c (with exclusion of $F4/80^+$ area) in WT→WT and KO→WT mice. Data combine 2 independent

experiments; total *n*=8 mice/condition). **g,h**, FACS quantification for tumour-associated $CD45^+$ leukocytes (**g**) or $CD45^+$ IgE^+ $CD49b^+$ $CD4^-CD45R^-$ basophils and $CD11b^+$ $SiglecF^+$ $Ly6C^{med}$ $F4/80^{low}$ $MHCII^-$ eosinophils (**h**) in WT→WT and KO→WT mice. Data combine 2 independent experiments; total *n*=8 mice/condition. **i,j**, FACS quantification (**i**) and gating strategy (**j**) for tumour-associated neutrophils selected from the main tumour cell population negative for 7AAD staining; tumour-associated neutrophils were then gated as CD11b and Ly6G double positive cells. Data combine 2 independent experiments; total *n*: WT→WT=11, KO→WT=10. **k**, $Ly6G^+$ tumour infiltration at day 9, day 13, and day 19 after LLC subcutaneous tumour injection in WT→WT and KO→WT mice. Data combine 2 independent experiments; total *n*=8 mice/condition. **l**, Morphometric quantification of leukocytes and macrophages on respectively CD45 and F480-stained lung sections from LLC tumour-bearing WT→WT or KO→WT mice. Data combine 2 independent experiments; total *n*=8 mice/condition. **m**, FACS quantification of $CD11b^+Ly6G^+$ neutrophils and $CD11b^+F4/80^+$ macrophages infiltrating metastatic lungs from LLC tumour-bearing WT→WT or KO→WT mice. Data combine 2 independent experiments; total *n*=8 mice/condition. *, $P<0.05$ versus WT→WT **(f,g,i,k-m)**; #, $P<0.05$ versus Tumour free (**a-d)**. All graphs show mean ± s.e.m.

Extended Data Figure 4. MET in neutrophils is required for their anti-tumour activity.

a,b, Western blot analysis (**a**) and relative densitometric analysis (**b**) for MET expression in BM neutrophils and monocytes upon reconstitution of WT recipient mice by WT or KO HSPCs transduced in vitro with an empty vector (Mrp8:Empty) or a vector expressing *Met* under the neutrophil-specific promoter Mrp8 (Mrp8:Met); tubulin was used as loading control. Western blots are representative of 3 repetitions on independent biological samples where each sample is the pool of neutrophils or monocytes isolated from 3 mice. Densitometric analysis has been performed on

these 3 Western blots. **c**, FACS analysis for GFP in circulating $Ly6G^+$ neutrophils or $CD115^+$ monocytes, harvested from the neutrophil-specific Mrp8:Cre line carrying separate expression of GFP because of an Internal Ribosome Entry Site (IRES) downstream the Mrp8-driven Cre gene. Data combine 2 independent experiments; total *n*=10 mice/condition. **d**, MET expression in neutrophils, monocytes, and macrophages harvested from Mrp8;$Met^{wt/wt}$ or Mrp8;$Met^{lox/lox}$ mice. Western blots are representative of 3 repetitions on independent biological replicates. **e,** FACS analysis for $CD11b^+Ly6G^+$ neutrophils in subcutaneous LLC tumours from Mrp8;$Met^{wt/wt}$ or Mrp8;$Met^{lox/lox}$. Data combine 2 independent experiments; total *n*: Mrp8;$Met^{wt/wt}$=10, Mrp8;$Met^{lox/lox}$=11. Western blot images in (**a,d**) have been cropped for presentation. Full scan images are shown in Supplementary Figure 1. *, $P<0.05$ versus Mrp8:Empty WT→WT (**b**), versus Mrp8;$Met^{wt/wt}$ (**e**); #, $P<0.05$ versus Mrp8:Empty WT→WT; $, $P<0.05$ versus Mrp8:Empty KO→WT**.** All graphs show mean ± s.e.m.

Extended Data Figure 5. Pharmacologic and genetic inhibition of MET prevents the recruitment of anti-tumoural neutrophils to several neoplastic tissues and inflammatory sites. **a,** Tumour weight of subcutaneous B16F10 melanomas in WT→WT and KO→WT mice. Data combine 2 independent experiments; total *n*: WT→WT=8, KO→WT=9. **b,c,** Total tumour weight (**b**) and metastatic index (**c**) in MMTV-PyMT mice reconstituted with WT or *Met* KO BM cells before tumour appearance (WT→PyMT and KO→PyMT mice, respectively). Data combine 3 independent experiments; total *n*: WT→PyMT=13, KO→PyMT=16. **d,e**, FACS quantification for $CD11b^+Ly6G^+$ neutrophils in T241 tumours harvested from WT→WT or KO→WT mice (**d**) or in in breast tumours spontaneously grown in WT→PyMT and KO→PyMT mice (**e**). Data combine 2 independent experiments; total *n*=10 mice/condition (**d**) or total *n*=8 mice/condition (**e**). **f-i,** Length measurement (**f**) and representative image (**g**) of the colon, as well as quantification of neutrophils

(**h**) and macrophages (**i**) on bowel sections, from WT→WT and KO→WT mice upon induction of chronic colitis compared to healthy control. Data combine 2 independent experiments; total *n*: healthy=5, WT→WT=12, KO→WT=15. **j,k**, Tumour weight (**j**) and metastatic mesenteric lymph nodes (**k**) 12 days after orthotopic injection of pancreatic Panc02 cancer cells in WT→WT and KO→WT mice. Data combine 2 independent experiments; total *n*=12/condition. **l**, Histological quantification of $Ly6G^+$ infiltrates in Panc02 pancreatic tumours harvested from WT→WT and KO→WT mice. Data combine 2 independent experiments; total *n*=12 mice/condition. **m,** Quantification of plasma HGF in tumour (TM)-free mice, in subcutaneous LLC or orthotopic Panc02 tumour-bearing mice. Data combine 2 independent experiments; total *n*: TM free=10, LLC=10, Panc02=8 biological replicates. **n**, Quantification of HGF in subcutaneous LLC or orthotopic Panc02 tumours. Data combine 2 independent experiments; total *n*: LLC=10, Panc02=8 biological replicates. **o,p**, Quantification of HGF in plasma (**o**) or in subcutaneous LLC tumours (**p**) from tumour-bearing WT→WT and KO→WT mice. Data are representative of 2 independent experiments using 5 mice/condition per experiment. **q**, Quantification of $Ly6G^+$ area on sections from B16F10 melanomas grown in C57BL/6 WT mice, daily treated with PF-04217903, INC280, JNJ-38877605, or vehicle as control. Data combine 2 independent experiments; total *n*: vehicle=14, PF-04217903=9, INC280=6, JNJ-38877605=4. **r,** Western blot analysis for MET in B16F10 melanoma cells after transduction with a lentiviral vector encoding scramble or mouse sh*Met* under a constitutive promoter; vinculin was used as loading control. Western blot is representative of 3 independent repetitions. Western blot images have been cropped for presentation. Full scan images are shown in Supplementary Figure 1. *, $P<0.05$ versus WT→WT (**a,d,h**), versus WT→PyMT (**b,e**), versus LLC (**m,n**), versus Vehicle (**q**); #, $P<0.05$ versus Healthy (**f,h,i**), versus TM free (**m**). Scale bar: 10 mm (**g**). All graphs show mean ± s.e.m.

Extended Data Figure 6. HGF is required for MET activation upon induction by TNF-α.

a, Gating strategy related to Fig. 3b to quantify MET expression in blood neutrophils from LLC-tumour (TM)-bearing mice and in TANs, where live cells were first gated as CD11b positive cells; this population was finally gated for Ly6G and MET in order to identify MET-expressing $Ly6G^+$ neutrophils. **b,c**, qRT-PCR for *MET* in mouse (b) and human (c) neutrophils after LPS or TNF-α stimulation. Data are representative of 3 independent experiments using 4 biological replicates/condition per experiment. **d,e**, qRT-PCR for *MET* expression in mouse (**b**) or human (**c**) neutrophils cultured in normoxia (21% O_2) or hypoxia (1% O_2). Data combine 2 independent experiments; total *n*=8 biological replicates/conditions per experiment. **f,g**, ELISA for total MET (**f**) and phospho-MET (**g**) from mouse neutrophils stimulated for 3 minutes with mock medium or HGF after an overnight incubation with or without TNF-α. Data combine 3 independent experiments; total *n*=6 biological replicates/conditions per experiment. **h**, HGF release by neutrophils stimulated with mock medium or TNF-α after 20 hours in culture. Data combine 2 independent experiments; total *n*=6 biological replicates/condition per experiment. **i**, qRT-PCR for *TNFA* in HUVEC upon stimulation with IL-1α compared to mock medium. Data combine 2 independent experiments; total *n*=4 biological replicates/condition. **j,** qRT-PCR for *Met* in mouse neutrophils co-cultured with HUVEC/NS or HUVEC/IL transduced with sh*TNFA* or scramble as control. Data are representative of 3 independent experiments where 3 different shRNA sequences were used; total *n*=4 biological replicates/condition per experiment. **k,l,** qRT-PCR for *Met* in WT, TNFR1, TNRF2 KO neutrophils upon co-culture with HUVEC/NS or HUVEC/IL (**k**), or after stimulation with conditioned medium (TCM) from LLC tumours (**l**). Data are representative of 2 independent experiments using 4 biological replicates/condition per experiment. **m**, qRT-PCR for *MET* in human neutrophils stimulated with A549-CCM in presence or absence of Enbrel or human IgGs as control. Data are representative of 2 independent experiments using 4 biological

replicates/condition per experiment. *, $P<0.05$ versus Mock (**b,c,i)**, versus TNF-α alone (**g)**, versus HUVEC/NS (**j)**, versus WT (**k,l),** versus A549-CCM **(m)**; #, $P<0.05$ versus untreated or HGF alone (**f,g)**, versus HUVEC/NS (**k**), versus Mock (**l,m)**. Graph shows mean ± s.e.m.

Extended Data Figure 7. *Met* deletion in neutrophils does not affect apoptosis.

a,b, Gating strategy of apoptotic WT (**a**) and *Met* KO (**b**) neutrophils in LLC tumours where single cells suspensions were firstly gated for physical parameters and then for CD11b and Ly6G in order to identify neutrophils as double positive cells; this population was finally gated for AnnexinV and 7AAD: AnnexinV$^+$ 7AAD$^-$ cells display early apoptotic neutrophils whereas AnnexinV$^+$ 7AAD$^+$ cells display late apoptotic neutrophils. **c**, Quantification of apoptotic WT and *Met* KO tumour-associated neutrophils measured by FACS. Data combine 2 independent experiments; total *n*=7 mice/condition. **d**, Quantification of apoptotic WT and *Met* KO neutrophils on LLC tumour sections by immunohistochemistry. Data combine 2 independent experiments; total *n:* WT→WT=7, KO→WT=6. **e**, FACS analysis for AnnexinV and 7AAD of WT or KO neutrophils incubated for 10 hours in presence or absence of LPS and HGF, alone or in combination. Data combine 2 independent experiments; total *n*=6 biological replicates/condition. #, $P<0.05$ versus untreated or HGF alone. Graph shows mean ± s.e.m.

Extended Data Figure 8. MET affects neither neutrophil basal migration nor polarization but it is required for neutrophil recruitment and cytotoxicity.

a, Quantification of Ly6G staining in ear-sections upon phorbol ester (TPA)-induced cutaneous rash in Mrp8;*Met*$^{wt/wt}$ and Mrp8;*Met*$^{lox/lox}$ mice. Data combine 2 independent experiments; total *n*=8 mice/condition. **b,** FACS analysis on peritoneal lavages for Ly6G$^+$ neutrophils or F4/80$^+$ macrophages in Mrp8;*Met*$^{wt/wt}$ and Mrp8;*Met*$^{lox/lox}$ mice 4 hours after intra-peritoneal injection of

sterile zymosan A. Data are representative of 2 independent experiments using 5 mice/condition per experiment. **c,d**, Quantification of F4/80 (**c**) and CD3 (**d**) stainings in ear-sections at baseline and upon TPA-induced cutaneous rash. Data combine 2 independent experiments; total *n*: WT→WT CTRL=22, KO→WT CTRL=15, WT→WT TPA=23, KO→WT CTRL=15 (**c**) or total *n*=8 mice/condition (**d**). **e,** FACS quantification of Mrp8;*Met*$^{wt/wt}$ and Mrp8;*Met*$^{lox/lox}$ neutrophils recruited into subcutaneous air pouches in response to HGF, CXCL1 or PBS. Data combine 2 independent experiments; total *n*=6 mice/condition. **f**, FACS quantification of WT neutrophil adhesion to quiescent HUVEC (HUVEC/NS) or activated HUVEC (HUVEC/IL) in presence or absence of HGF. Data are representative of 2 independent experiments using 4 biological replicates/condition per experiment. **g,h,** FACS quantification of WT and *Met* KO neutrophils migrated through a bare porous filter (*i.e.,* in absence of HUVEC) towards HGF (**g**) or tumour conditioned medium (TCM) (**h**). Data are representative of 2 independent experiments using 3 biological replicates/condition per experiment. **i**, Gene expression profile for N1 and N2 markers in neutrophils sorted from LLC tumours grown in WT→WT or KO→WT mice. Data are representative of 3 independent experiments using 4 mice/condition per experiment. **j,** Cytotoxicity of WT and KO tumour-associated neutrophils against T241 cells in absence or presence of the NO synthase inhibitor L-NMMA. Data are representative of 3 independent experiments using 3 biological replicates/condition per experiment. **k,** FACS quantification of DAF-FM-positive circulating neutrophils after co-culture with LLC cancer cells as a readout of NO production in absence or presence of HGF. Data are representative of 4 independent experiments using 3 biological replicates/condition per experiment. **l,** Quantification of LLC cancer cell killing by WT and KO neutrophils (isolated from the blood of tumour-bearing mice), stimulated with HGF alone or in presence of L-NMMA. Data are representative of 2 independent experiments using *n*=12 biological replicates/condition per experiment. **m**, Blood neutrophils in WT→WT and KO→WT

mice treated with neutrophil-depleting Ly6G antibody or rat IgG as control. Data combine 2 independent experiments; total *n*=16/condition. *, *P*<0.05 versus Mrp8;*Met*$^{wt/wt}$ (**a**,**b)**, versus Mrp8;*Met*$^{wt/wt}$ + HGF (**e)**, versus HUVEC/NS (**f)**, versus WT→WT untreated (**j)**, versus WT→WT HGF (**k**,**l);** #, *P*<0.05 versus CTRL (**c**,**d)**, versus PBS (**e)**, versus Mock (**f,h)**, versus WT→WT untreated (**j-l**), versus IgG **(m)**; $, *P*<0.05 versus WT→WT HGF (**m**). All graphs show mean ± s.e.m.

Extended Data Table 1. Blood count in Tie2;*Met*$^{wt/wt}$ or Tie2;*Met*$^{lox/lox}$ tumour free mice.

The values show the hematological parameters (mean ± s.e.m.) in tumour free Tie2;*Met*$^{wt/wt}$ and Tie2;*Met*$^{lox/lox}$ mice. Data combine 2 independent experiments; total *n*=10/condition. Abbreviations: white blood cell (WBC), neutrophil (NEU), lymphocyte (LYM), monocyte (MON), eosinophil (EOS), basophil (BAS), red blood cell (RBC), hematocrit (HCT), mean cell hemoglobin concentration (MCHC), platelet (PLT).

Extended Data Table 2. Blood count in WT→WT and KO→WT tumour free or tumour bearing mice.

The values show the hematological parameters (mean ± s.e.m.) in tumour free or in LLC-tumour bearing (21 days) WT→WT and KO→WT chimeric mice. Data combine 2 independent experiments; total *n*=10/condition. Abbreviations: white blood cell (WBC), neutrophil (NEU), lymphocyte (LYM), monocyte (MON), eosinophil (EOS), basophil (BAS), red blood cell (RBC), hematocrit (HCT), mean cell hemoglobin concentration (MCHC), platelet (PLT).

Fig. 1

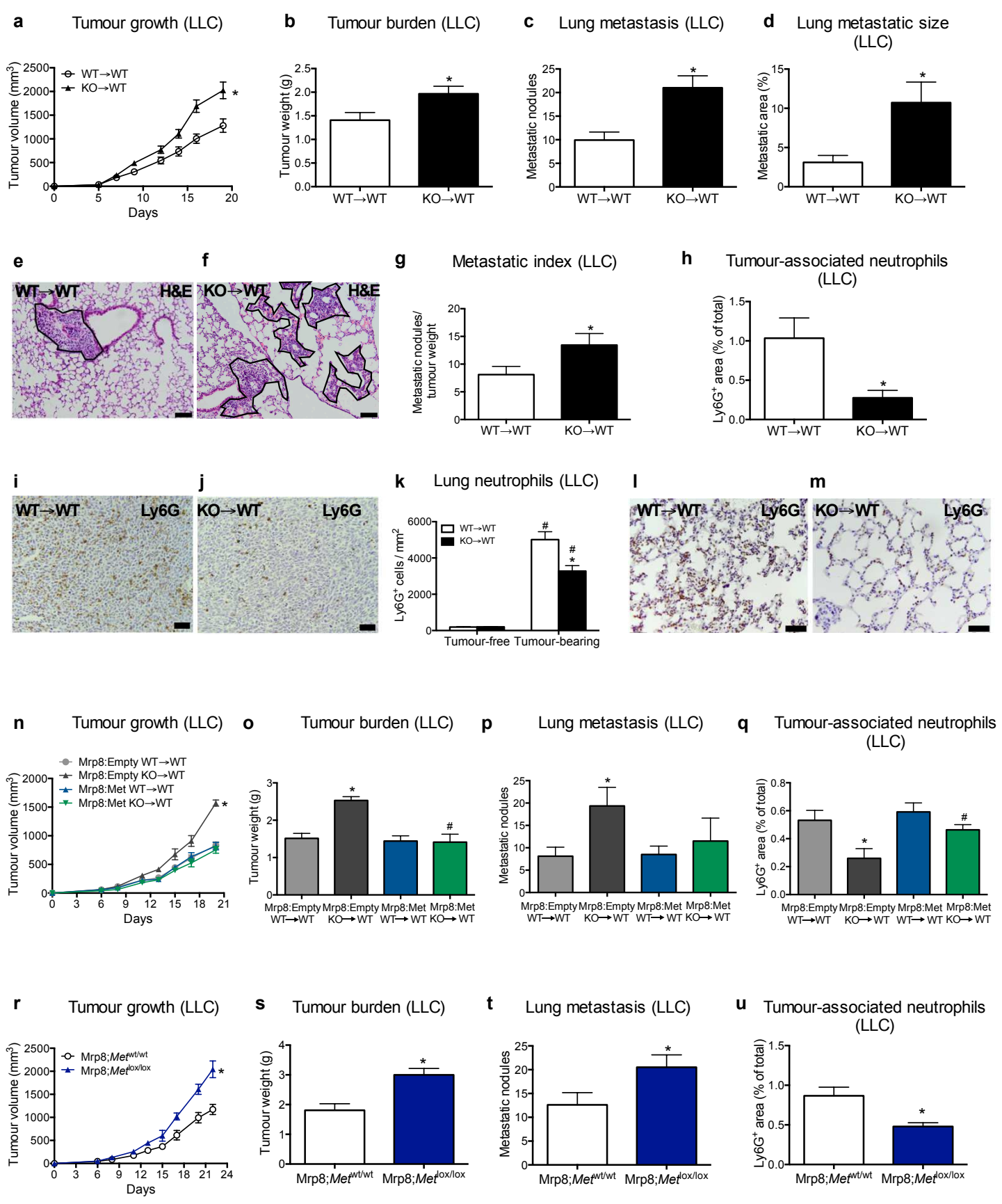
a
Tumour growth (LLC)
Tumour volume (mm3)
WT→WT
KO→WT
Days
b
Tumour burden (LLC)
Tumour weight (g)
c
Lung metastasis (LLC)
Metastatic nodules
d
Lung metastatic size (LLC)
Metastatic area (%)
e
WT→WT
H&E
f
KO→WT
H&E
g
Metastatic index (LLC)
Metastatic nodules/ tumour weight
h
Tumour-associated neutrophils (LLC)
Ly6G+ area (% of total)
i
WT→WT
Ly6G
j
KO→WT
Ly6G
k
Lung neutrophils (LLC)
Ly6G+ cells / mm2
Tumour-free
Tumour-bearing
l
WT→WT
Ly6G
m
KO→WT
Ly6G
n
Tumour growth (LLC)
Mrp8:Empty WT→WT
Mrp8:Empty KO→WT
Mrp8:Met WT→WT
Mrp8:Met KO→WT
Tumour volume (mm3)
Days
o
Tumour burden (LLC)
Tumour weight (g)
Mrp8:Empty WT→WT
Mrp8:Empty KO→WT
Mrp8:Met WT→WT
Mrp8:Met KO→WT
p
Lung metastasis (LLC)
Metastatic nodules
q
Tumour-associated neutrophils (LLC)
Ly6G+ area (% of total)
r
Tumour growth (LLC)
Mrp8;Metwt/wt
Mrp8;Metlox/lox
Tumour volume (mm3)
Days
s
Tumour burden (LLC)
Tumour weight (g)
t
Lung metastasis (LLC)
Metastatic nodules
u
Tumour-associated neutrophils (LLC)
Ly6G+ area (% of total)

Fig. 2

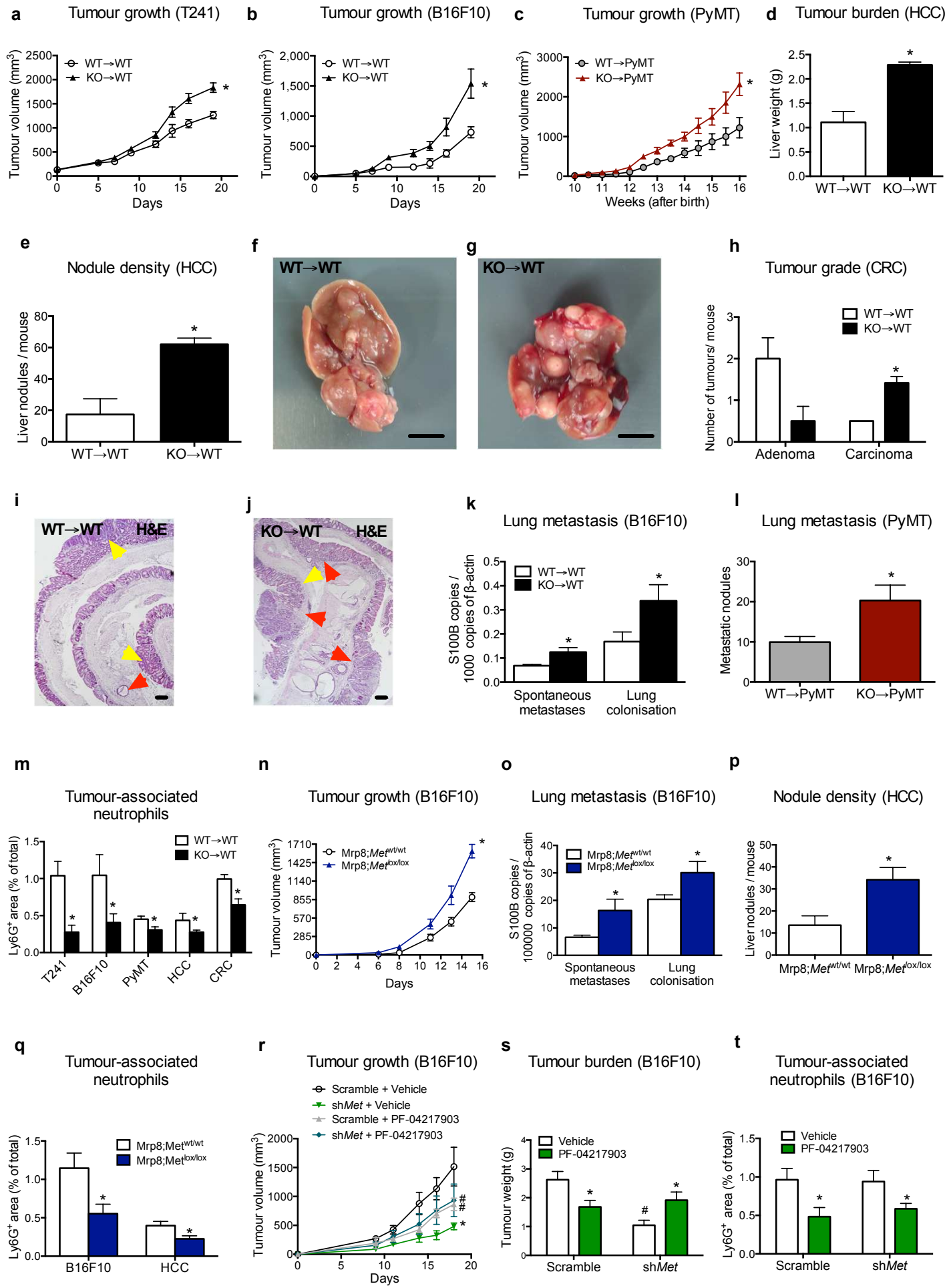
a
Tumour growth (T241)
Tumour volume (mm3)
WT→WT
KO→WT
Days
b
Tumour growth (B16F10)
Tumour volume (mm3)
WT→WT
KO→WT
Days
c
Tumour growth (PyMT)
Tumour volume (mm3)
WT→PyMT
KO→PyMT
Weeks (after birth)
d
Tumour burden (HCC)
Liver weight (g)
WT→WT
KO→WT
e
Nodule density (HCC)
Liver nodules / mouse
WT→WT
KO→WT
f
WT→WT
g
KO→WT
h
Tumour grade (CRC)
Number of tumours/ mouse
WT→WT
KO→WT
Adenoma
Carcinoma
i
WT→WT
H&E
j
KO→WT
H&E
k
Lung metastasis (B16F10)
S100B copies / 1000 copies of β-actin
WT→WT
KO→WT
Spontaneous metastases
Lung colonisation
l
Lung metastasis (PyMT)
Metastatic nodules
WT→PyMT
KO→PyMT
m
Tumour-associated neutrophils
Ly6G+ area (% of total)
WT→WT
KO→WT
T241
B16F10
PyMT
HCC
CRC
n
Tumour growth (B16F10)
Tumour volume (mm3)
Mrp8;Metwt/wt
Mrp8;Metlox/lox
Days
o
Lung metastasis (B16F10)
S100B copies / 100000 copies of β-actin
Mrp8;Metwt/wt
Mrp8;Metlox/lox
Spontaneous metastases
Lung colonisation
p
Nodule density (HCC)
Liver nodules / mouse
Mrp8;Metwt/wt
Mrp8;Metlox/lox
q
Tumour-associated neutrophils
Ly6G+ area (% of total)
Mrp8;Metwt/wt
Mrp8;Metlox/lox
B16F10
HCC
r
Tumour growth (B16F10)
Scramble + Vehicle
shMet + Vehicle
Scramble + PF-04217903
shMet + PF-04217903
Tumour volume (mm3)
Days
s
Tumour burden (B16F10)
Tumour weight (g)
Vehicle
PF-04217903
Scramble
shMet
t
Tumour-associated neutrophils (B16F10)
Ly6G+ area (% of total)
Vehicle
PF-04217903
Scramble
shMet

Fig. 3

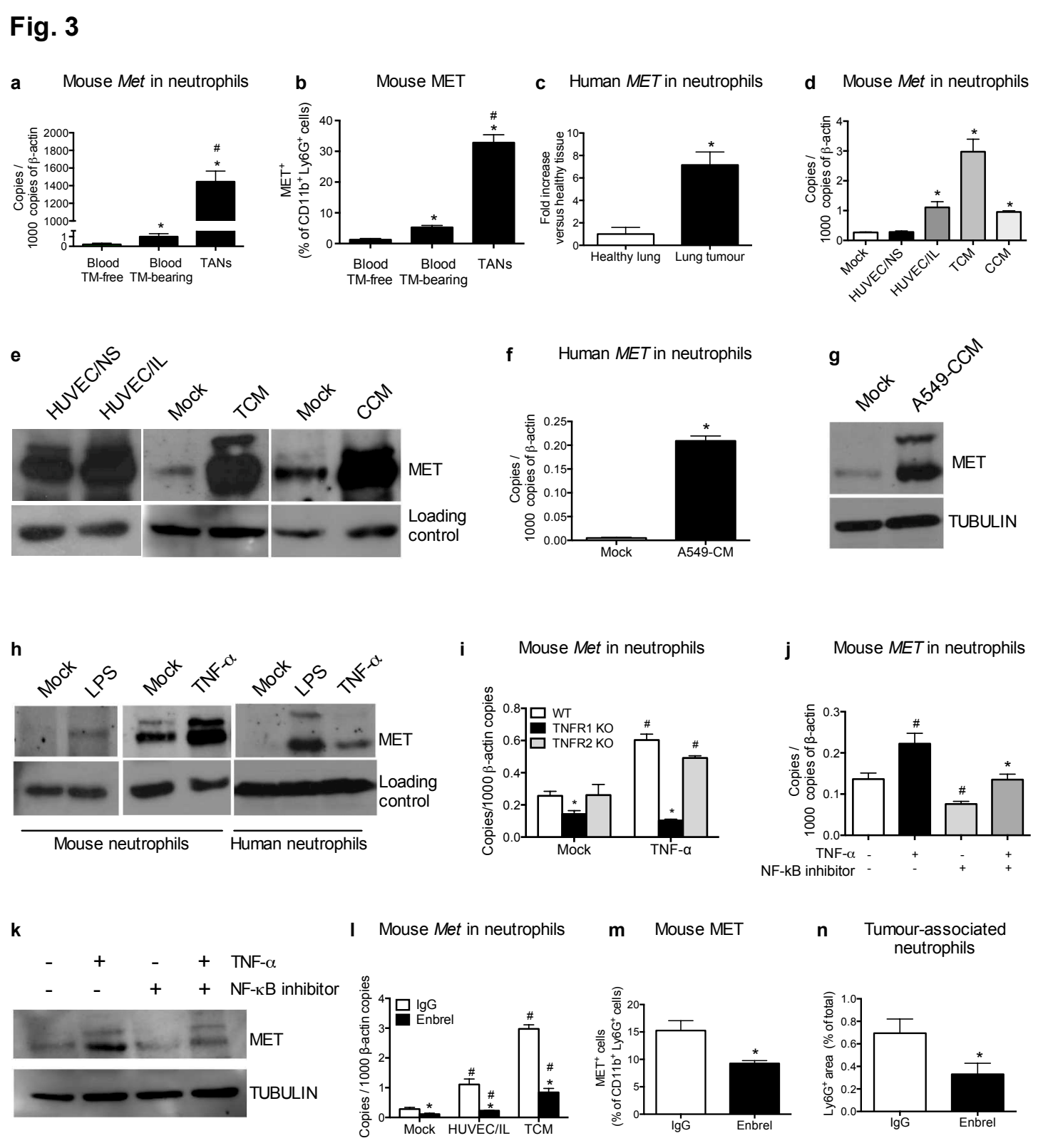
a
Mouse Met in neutrophils
Copies / 1000 copies of β-actin
Blood TM-free
Blood TM-bearing
TANs
b
Mouse MET
MET+ (% of CD11b+Ly6G+ cells)
c
Human MET in neutrophils
Fold increase versus healthy tissue
Healthy lung
Lung tumour
d
Mouse Met in neutrophils
Mock
HUVEC/NS
HUVEC/IL
TCM
CCM
e
HUVEC/NS
HUVEC/IL
Mock
TCM
Mock
CCM
MET
Loading control
f
Human MET in neutrophils
Mock
A549-CM
g
Mock
A549-CCM
MET
TUBULIN
h
Mock
LPS
Mock
TNF-α
Mock
LPS
TNF-α
MET
Loading control
Mouse neutrophils
Human neutrophils
i
Mouse Met in neutrophils
Copies/1000 β-actin copies
WT
TNFR1 KO
TNFR2 KO
Mock
TNF-α
j
Mouse MET in neutrophils
Copies / 1000 copies of β-actin
TNF-α
NF-kB inhibitor
k
TNF-α
NF-κB inhibitor
MET
TUBULIN
l
Mouse Met in neutrophils
Copies / 1000 β-actin copies
IgG
Enbrel
Mock
HUVEC/IL
TCM
m
Mouse MET
MET+ cells (% of CD11b+Ly6G+ cells)
IgG
Enbrel
n
Tumour-associated neutrophils
Ly6G+ area (% of total)
IgG
Enbrel

Fig. 4

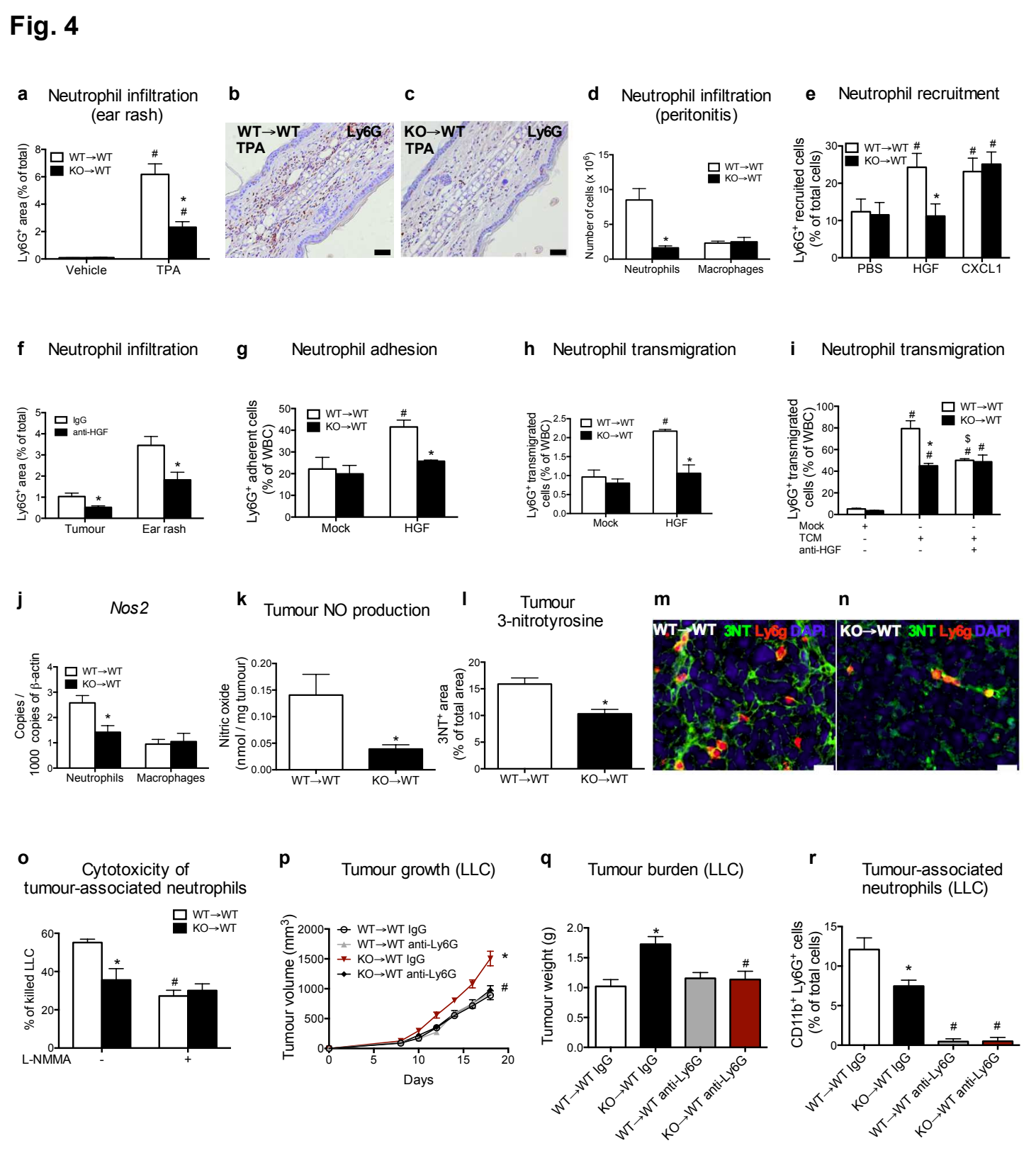
a
Neutrophil infiltration (ear rash)
Ly6G+ area (% of total)
WT→WT
KO→WT
Vehicle
TPA
b
WT→WT TPA
Ly6G
c
KO→WT TPA
Ly6G
d
Neutrophil infiltration (peritonitis)
Number of cells (x 10^6)
Neutrophils
Macrophages
e
Neutrophil recruitment
Ly6G+ recruited cells (% of total cells)
PBS
HGF
CXCL1
f
Neutrophil infiltration
Ly6G+ area (% of total)
IgG
anti-HGF
Tumour
Ear rash
g
Neutrophil adhesion
Ly6G+ adherent cells (% of WBC)
Mock
HGF
h
Neutrophil transmigration
Ly6G+ transmigrated cells (% of WBC)
i
Neutrophil transmigration
Ly6G+ transmigrated cells (% of WBC)
Mock
TCM
anti-HGF
j
Nos2
Copies / 1000 copies of β-actin
k
Tumour NO production
Nitric oxide (nmol / mg tumour)
l
Tumour 3-nitrotyrosine
3NT+ area (% of total area)
m
WT→WT 3NT Ly6g DAPI
n
KO→WT 3NT Ly6g DAPI
o
Cytotoxicity of tumour-associated neutrophils
% of killed LLC
L-NMMA
p
Tumour growth (LLC)
Tumour volume (mm3)
WT→WT IgG
WT→WT anti-Ly6G
KO→WT IgG
KO→WT anti-Ly6G
Days
q
Tumour burden (LLC)
Tumour weight (g)
r
Tumour-associated neutrophils (LLC)
CD11b+ Ly6G+ cells (% of total cells)